



HAL
open science

Localization of correlated moving sources from numerical flyover scenarios

Hugo Demontis, Emmanuel Julliard

► **To cite this version:**

Hugo Demontis, Emmanuel Julliard. Localization of correlated moving sources from numerical flyover scenarios. INTERNOISE 2024, Aug 2024, Nantes, France. hal-04704027

HAL Id: hal-04704027

<https://hal.science/hal-04704027v1>

Submitted on 20 Sep 2024

HAL is a multi-disciplinary open access archive for the deposit and dissemination of scientific research documents, whether they are published or not. The documents may come from teaching and research institutions in France or abroad, or from public or private research centers.

L'archive ouverte pluridisciplinaire **HAL**, est destinée au dépôt et à la diffusion de documents scientifiques de niveau recherche, publiés ou non, émanant des établissements d'enseignement et de recherche français ou étrangers, des laboratoires publics ou privés.

Localization of correlated moving sources from numerical flyover scenarios

Hugo Demontis¹

DAAA, ONERA, Institut Polytechnique de Paris
29 avenue de la Division Leclerc, 92320 Châtillon, France

Emmanuel Julliard²

Airbus Operations S.A.S, Acoustics Department
316 route de Bayonne, 31300 Toulouse, France

ABSTRACT

The noise emissions during flyover test can be analyzed with a phased microphone array placed on the ground. If the flight path is known, an acoustic imaging technique is then used to map the sound pressure over the fuselage, in order to locate the most emergent aeroacoustic sources. Most of the dedicated array techniques assume a spatial distribution of uncorrelated equivalent sources to be sought. This paper deals with the localization of correlated moving sources, and demonstrates the effectiveness of an uncorrelated-based deconvolution technique for this purpose. The technique is applied on synthetic data from three different numerical scenarios, including a simplistic configuration of an overflying aircraft, which involve a small number of sparse, correlated monopoles in motion.

1. INTRODUCTION

As a duty to airport communities, embodied within stricter noise regulations imposed by airworthiness authorities, the noise performance of next generations of aircraft is of major interest, and requires more advanced noise measurement systems. In this context, phased microphone array processing can complement existing standard measurement protocols. The tedious part of this approach is to synchronize the acquisition from a thousand of sensors on the ground with the in-board aircraft trajectography system. Thus, any acoustic imaging techniques, like time-domain conventional beamforming, can be used to locate the emergent aeroacoustic noise sources. Recent research has focused on the adaptation of existing high-resolutive techniques to take into account of the displacement of the sound sources. The extensions of DAMAS [1], CLEAN [2] or the functional beamforming algorithm [3], have improved the spatial resolution and the dynamic range of the resulted acoustic cartography along the fuselage of the aircraft.

Most of the microphones array techniques model the sources to be sought as a spatial distribution of uncorrelated monopoles. They become inaccurate in case of non-compact sources with anisotropic directivity effects. This is particularly true for aircraft noise analysis, where high

¹hugo.demontis@onera.fr

²emmanuel.julliard@airbus.com

sound levels with important directivities are generated by the airframe, the landing gears or the jet engine. For wind tunnel applications, DAMAS-C and CMF-C are two techniques which ease the restauration of the cross spectral matrix of this type of sources [4]. However, they have not been yet extended to flyover applications.

This paper deals with the localization of correlated moving sources. It provides preliminary results for the implementation of new correlation-based techniques dedicated to flyover measurements. In this context, we propose to evaluate the performance of the deconvolution technique exposed in [1], which is based on an uncorrelated sources model. The theoretical aspects of the technique, in particular the time-frequency formulation of beamforming, are developed first. It is then applied on synthetic data from different numerical scenarios. Each scenario considers a small set of sparse and correlated monopoles, and varies according to the trajectory, the number and the nature (tonal or broadband) of these monopoles. While the first two scenarios are more academic configurations, the third attempt to reproduce the noise measurements of a simplified flyover using representative trajectography.

2. ARRAY TECHNIQUE

2.1. Direct model

In the following sections, all the coordinates vectors refer to the same static coordinate system on the ground. The flight path of the aircraft is tracked over time, for instance using a global positioning system, and so its trajectory is precisely known at discrete emission times t_e . During the flyover, an array of M fixed microphones, each located on the ground at \mathbf{x}_m , measures the noise from a set of N sources moving with the aircraft. The measurements have to be synchronized with the trajectory. By denoting $\mathbf{x}_n(t_e)$ and $\mathbf{U}_n(t_e)$ respectively the instantaneous location and velocity of the n^{th} source, the emission angle relative to the trajectory at time t_e is given by the following scalar product:

$$\theta_{mn}(t_e) = \frac{\mathbf{x}_m - \mathbf{x}_n(t_e)}{|\mathbf{x}_m - \mathbf{x}_n(t_e)|} \cdot \frac{\mathbf{U}_n(t_e)}{|\mathbf{U}_n(t_e)|} \quad (1)$$

For medium-range propagation distances between sources and microphones, the convection of sound waves by the wind could be significant. The acoustic propagation is therefore modelled in an infinite uniform low-speed flow above the ground, with c_0 the sound celerity and \mathbf{M}_0 the Mach vector of the wind. The pressure signal $s_n(t_e)$ emitted by the n^{th} source reaches the m^{th} static microphone after the propagation delay:

$$\tau_{mn}(t_e) = \frac{-\mathbf{M}_0 \cdot (\mathbf{x}_m - \mathbf{x}_n(t_e)) + \sqrt{[\mathbf{M}_0 \cdot (\mathbf{x}_m - \mathbf{x}_n(t_e))]^2 + \beta^2 |\mathbf{x}_m - \mathbf{x}_n(t_e)|^2}}{c_0 \beta^2}, \quad (2)$$

with $\beta^2 = 1 - |\mathbf{M}_0|^2$. Under the hypothesis of a moving monopole, and from Equation 1 and Equation 2, a model of received signal is:

$$p_m(t_e + \tau_{mn}(t_e)) = \frac{s_n(t_e)}{|\mathbf{x}_m - \mathbf{x}_n(t_e)| [1 - M_n(t_e) \cos \theta_{mn}(t_e)]^2}, \quad (3)$$

where $M_n(t_e) = |\mathbf{U}_n(t_e)|/c_0$ is the Mach number of the source. The delay in Equation 2 varies with the source-to-microphone distance and thus, the resulting reception times $t_e + \tau_{mn}(t_e)$ are not evenly spaced. This induces the so-called Doppler signature, due to the motion of the source relative to the fixed receiver.

2.2. Beamforming

Beamforming is used to locate the emergent noise sources along the aircraft, and reconstruct their acoustic signature. The approach used in this paper follows in part the formulation by

Cousson [2], which has been adapted in [5] to flyover applications. The main steps of the algorithm are summarized below. Beamforming is applied blindly along a discrete grid of size I , moving with the aircraft and delimiting its fuselage. The i^{th} node of the grid can be located at $\mathbf{x}_i(t_e)$, and represents an equivalent noise source for which the beamformed signal writes:

$$s_i(t_e) = \sum_{m=1}^M \frac{p_m(t_e + \tau_{mi}(t_e))}{|\mathbf{x}_m - \mathbf{x}_i(t_e)| [1 - M_n(t_e) \cos \theta_{mi}(t_e)]^2} \quad (4)$$

Here, the signal s_i derives from the dedopplerization of the measurements p_m by selecting the pressure bins at corresponding reception times $t_e + \tau_{mi}(t_e)$ defined by Equation 2 [6]. As these reception times do not generally coincide with the sampling period of the measurements, data must be interpolated to avoid large errors in pressure amplitudes. In our case, a natural cubic spline interpolation scheme is used. When $\mathbf{x}_i(t_e) = \mathbf{x}_n(t_e)$, the estimate from Equation 4 equals the true emission $s_n(t_e)$.

Let $\hat{s}_i(\omega)$ the Fourier Transform of s_i at angular frequency ω . The power spectral density vector $\mathbf{b} \in \mathbb{R}^{I \times 1}$ of the equivalent sources is given by:

$$b_i(\omega) = \hat{s}_i(\omega) \overline{\hat{s}_i(\omega)}, \quad \forall i = 1 \dots I \quad (5)$$

with $\overline{(\cdot)}$ the complex-conjugate operator. In practice, the vector \mathbf{b} is computed using a Welch's periodogram technique. The dedopplerized source signals are evaluated for a number K of emission frames, with a percent of overlap between successive frames. The duration of a single frame depends on the targeted frequency resolution of the equivalent sources. The spectra $\hat{s}_i^{(k)}$ are then averaged over the frames. The Equation 5 becomes:

$$b_i(\omega) \approx \frac{1}{K} \sum_{k=1}^K \hat{s}_i^{(k)}(\omega) \overline{\hat{s}_i^{(k)}(\omega)} \quad (6)$$

2.3. Deconvolution

Deconvolution refers to all the techniques used to improve the resolution of acoustic imaging by the direct clean of the beamforming output given by Equation 6. These techniques rely on the knowledge of the sensing matrix:

$$\mathbf{H}(\omega_D) = |\mathbf{G}^H(\omega_D) \mathbf{G}(\omega_D)|^2 \quad (7)$$

Each column of $\mathbf{H} \in \mathbb{R}^{I \times I}$ is the point spread function (PSF) of the array for the i^{th} equivalent source of the focusing grid, and links to the Green's function matrix $\mathbf{G} \in \mathbb{C}^{M \times I}$. For the specific case of point-like moving monopole, the Green's function between the i^{th} equivalent source and the m^{th} microphone at angular Doppler-shifted frequency ω_D writes as follow [1]:

$$G_{mi}(\omega_D) = \frac{e^{-jk_D |\mathbf{x}_m - \mathbf{x}_i(t_e)|}}{|\mathbf{x}_m - \mathbf{x}_i(t_e)| [1 - M_i(t_e) \cos \theta_{mi}(t_e)]^2}, \quad (8)$$

with $k_D = \omega_D / c_0$ the wavenumber.

In the present paper, the deconvolution aims at finding the vector $\mathbf{s} \in \mathbb{R}^{I \times 1}$, solution of the linear system

$$\mathbf{H}\mathbf{s} = \mathbf{b}, \quad (9)$$

subject to the non-negativity constraint $s_i \geq 0, \forall i = 1 \dots I$. This ensures to converge to the physical power of the sources. In this work, the Equation 9 is solved in the non-negative least-square sense using the Lawson-Hansen algorithm [7].

3. NUMERICAL SCENARIOS

3.1. General setup

The general configuration for the three numerical cases is shown in Figure 1. The propagation in altitude occurs at sound celerity $c_0 = 343m/s$ and low wind speed $|\mathbf{U}_0| = 10m/s$. A cross-shaped array of $M = 250$ microphones is placed on ground [8]. Time-resolved pressure data on microphones are finally synthesized according the direct model in Equation 3. Introducing $\mathbf{T}(\rho) \in \mathbb{R}^{3 \times 3}$ the source covariance matrix, we can control the degree of correlation between sources by tuning a single parameter ρ [4]. Analysis are done at emission angle $\theta_{ms} = 90^\circ$, the index m for the central microphone of the array and the index s for a reference point of the moving focusing grid.

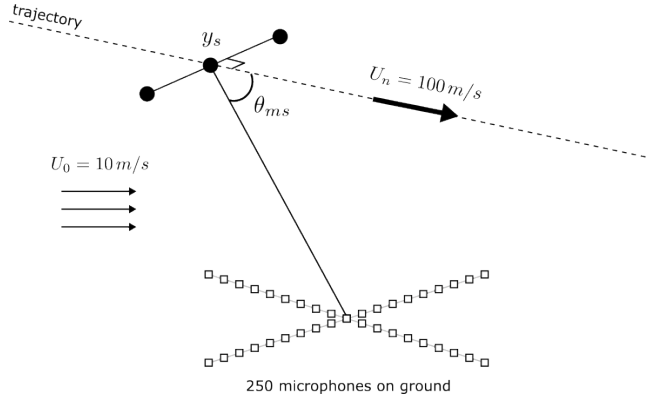


Figure 1: Sketch of the general simulated configuration.

3.2. Three uncorrelated sources

First, the case of three broadband uncorrelated monopoles ($\rho = 0$) is considered. The simulated sources follow the same approach trajectory above the array at constant speed $|\mathbf{U}_n| = 100m/s$ and slope $\phi = -3^\circ$. They are aligned along Y-axis, and spaced by 5 meters. During the flight, each one generates a zero-mean gaussian noise with power spectral density amplitude of $1Pa^2/Hz$.

For the localization, the equivalent sources are sought along a one-dimensional regular grid passing through the three sources, and divided into $I = 201$ between $y_s = -10$ and $y_s = 10$ meters. The vector \mathbf{b} is averaged over $K = 31$ blocks, with a Hanning temporal window and 50% of overlap. The frequency resolution is set to 32Hz. No spatial apodization of the array has been considered in the computation.

The Figure 2 shows the beamformed and the deconvolved acoustic maps obtained for this first simulation. The vertical dashed lines indicate the true source locations. As expected, and because the source model is suited for this scenario, the peaks of amplitude are found at the three locations of the uncorrelated sources. It is not possible to separate them up to 300Hz because of the wider beamwidth of the array on this frequency range.

3.3. Three correlated sources

Then, a case similar to that of Section 2 is considered, except that the three broadband monopoles are now correlated ($\rho = 0.8$). The same parameters are chosen to compute the vector \mathbf{b} .

The Figure 3 shows the beamformed and the deconvolved acoustic maps obtained for this second simulation. They have to be compared with the references in Figure 2. Here, the deconvolution technique is also able to correctly locate the three correlated sources. Note the more pronounced sidelobes above 2000Hz, which suggest that the algorithm does not fully remove the PSFs from the dirty map, and can emphasize significant temporal interactions between the sources. Moreover, the localization is now impaired at low frequencies up to 1000Hz.

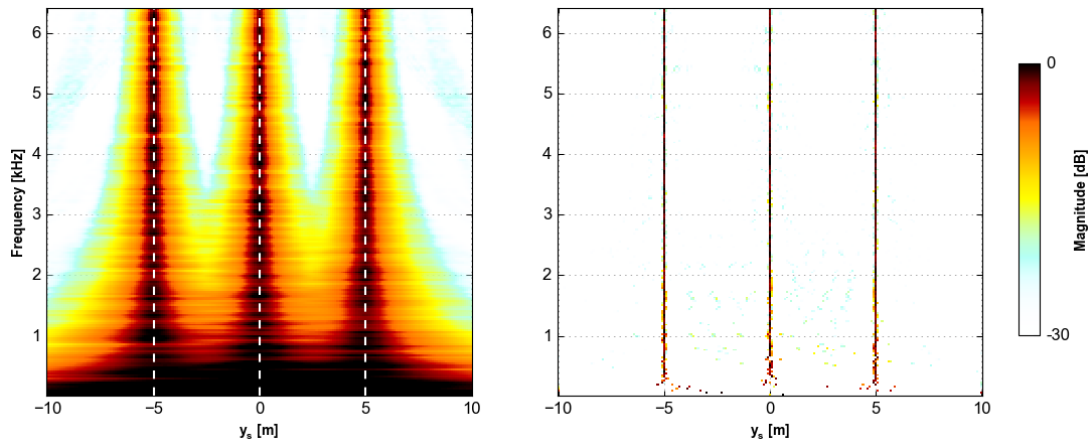


Figure 2: Space-frequency acoustic maps for the three uncorrelated sources ($\rho = 0$) using beamforming (on left) and deconvolution (on right).

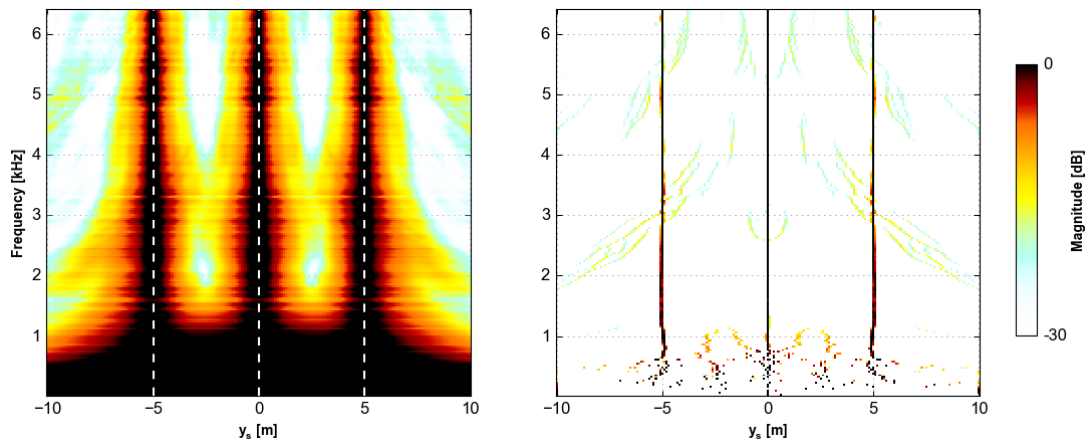


Figure 3: Space-frequency acoustic maps for the three correlated sources ($\rho = 0.8$) using beamforming (on left) and deconvolution (on right).

3.4. Simplified aircraft noise

Finally, we consider the case of several monopoles superimposed on the noisiest parts of an aircraft. This simulation derives directly from the proposal in [5]. It comprises three correlated broadband monopoles on the landing gears, and two tonal monopoles, respectively at 440Hz and 880Hz, on the fan engine noise, see Figure 4. Here, only the correlation among the broadband sources is imposed ($\rho = 0.6$).

For the localization, a two-dimensional grid of $I = 2601$ equivalent sources delimits the wingspan of the aircraft, with a resolution of 1 meters along the X- and Y-axis. The vector \mathbf{b} is averaged over $K = 39$ blocks, with a Hanning temporal window and 50% of overlap. The frequency resolution is set to 20Hz.

The Figure 5 shows the deconvolved acoustic maps obtained for the modelled aircraft. The resulting maps are integrated over three third-octave bands at 400Hz, 800Hz and 1250Hz. All five monopoles are visible. For bands 400Hz and 800Hz, the strong emergence of the tonal sources, in addition to the poor dynamic range of the array, could explain why the broadband sources can't be correctly seen. This issue has not been observed with the simulation from [5]. Note also, at 1250Hz, the interaction between the two sources placed on the rear landing gears. Their theoretical PSFs seems to cross at these locations, creating symmetric ghost sources which pollute the acoustic map.

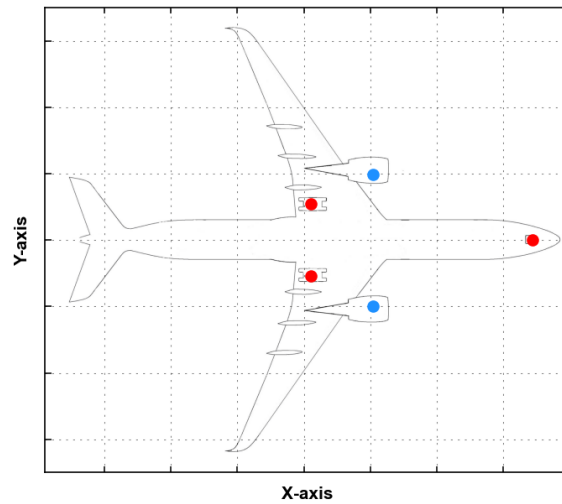


Figure 4: Simulated tonal (blue dot) and broadband (red dot) monopoles along the aircraft

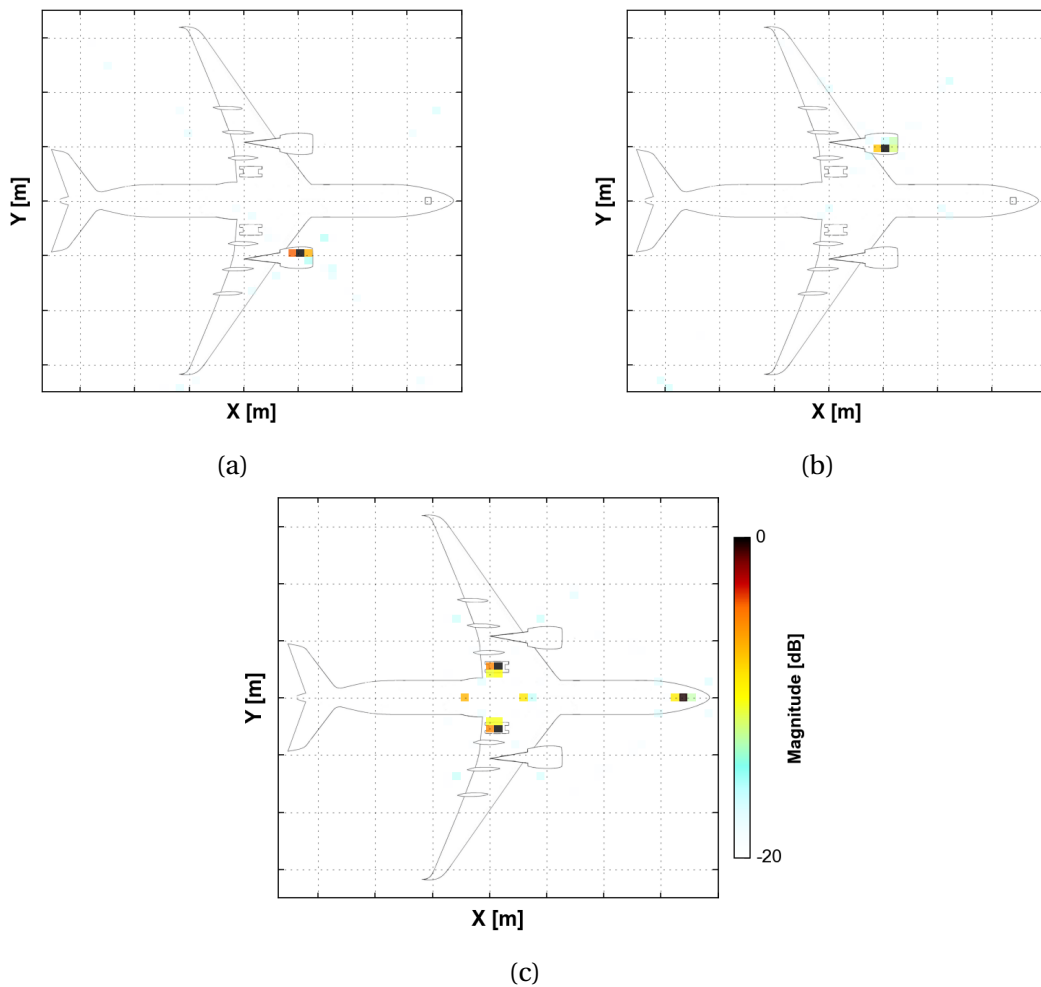


Figure 5: Third-octave integrated deconvolved maps for the simplified aircraft at (a) 400Hz, (b) 800Hz and (c) 1250Hz. The dynamic range and colorbar is the same for the three figures.

4. CONCLUSION

In this paper, the performance of an uncorrelated-based deconvolution technique has been demonstrated for dealing with the complex case of correlated moving acoustic sources. It has

been applied to synthetic data from ground-truth simplistic numerical scenarios. The results showed that the deconvolution is capable of locating moving sources that may or may not be correlated. This is true in the mid- and high-range frequencies, but less so for low frequencies due to the limited spatial resolution of the array. This motivates the adaptation of existing correlation-based deconvolution techniques, such as DAMAS-C or CLEAN-SC, to overcome this drawback.

ACKNOWLEDGEMENTS

The authors are grateful to Airbus, especially to Emmanuel Julliard, For providing relevant inputs for the computation. This work was carried out in the framework of the MAMBO project, supported by the French Civil Aviation Agency (DGAC), the “France Relance” national recovery plan, and the ”Nextgeneration EU” european recovery plan.

REFERENCES

1. V. Fleury and P. Malbequi. Slat noise assessment from Airbus A340 flyover phased-array microphone measurements. *AIAA Journal*, 51(7):1667–1674, 2013.
2. R. Cousson, Q. Leclere, M.A. Pallas, and M. Berengier. A time domain CLEAN approach for the identification of acoustic moving sources. *Journal of Sound and Vibration*, 443:47–62, 2019.
3. R. Merino-Martínez, M. Snellen, and D.G. Simons. Functional beamforming applied to imaging of flyover noise on landing aircraft. *Journal of Aircraft*, 53(6):1830–1843, 2016.
4. T. Yardibi, J. Li, P. Stoica, N. Zawodny, and L. Cattafesta III. Sparsity constrained deconvolution approaches for acoustic source mapping. *The Journal of the Acoustical Society of America*, 123(5):2631–2642, 2008.
5. R. Leiba, H. Demontis, Q. Leclere, S. Fauqueux, and E. Julliard. Acoustic imaging on aircraft flyover tests: Comparing CLEAN-T to DAMAS-MS. In *Proceedings of the 10th Convention of the European Acoustics Association, Forum Acusticum 2023*, Roma, Italy, September 2023.
6. B. Barkisow and W.F. King. On removing the doppler frequency shift from array measurements of railway noise. *Journal of Sound and Vibration*, 120(1):190–196, 1988.
7. G. Chardon, J. Picheral, and F. Ollivier. Theoretical analysis of the DAMAS algorithm and efficient implementation of the covariance matrix fitting method for large-scale problems. *Journal of Sound and Vibration*, 508:116208, 2021.
8. G. Elias. Source localization with a two-dimensional focused array: optimal signal processing for a cross-shaped array. In *Proceedings of INTER-NOISE 95*, pages 1175–1178, Newport Beach, California, USA, July 1995.